



Abnormal brown adipose tissue mitochondrial structure and function in IL10 deficiency



José C. de-Lima-Júnior^{a,b,1}, Gabriela F. Souza^{a,b,1}, Alexandre Moura-Assis^{a,b,1}, Rodrigo S. Gaspar^{b,c}, Joana M. Gaspar^{a,b,1}, Andréa L. Rocha^d, Danilo L. Ferrucci^{e,f}, Tanes I. Lima^{b,d}, Sheila C. Victório^{a,b,1}, Ivan L.P. Bonfante^g, Claudia R. Cavaglieri^g, José C. Pareja^h, Sérgio Q. Brunettoⁱ, Celso D. Ramos^{b,j}, Bruno Geloneze^{b,h}, Marcelo A. Mori^d, Leonardo R. Silveira^{b,d}, Gesmar R.S. Segundo^k, Eduardo R. Ropelle^{b,c}, Lício A. Velloso^{a,b,*,1}

^a Laboratory of Cell Signaling, Department of Internal Medicine, University of Campinas, Campinas, São Paulo 13084-970, Brazil

^b Obesity and Comorbidities Research Center, University of Campinas, Campinas, São Paulo 13084-970, Brazil

^c CEPECE - Research Center of Sport Sciences, School of Applied Sciences, University of Campinas, Limeira, SP, Brazil

^d Department of Biochemistry and Tissue Biology, Institute of Biology, University of Campinas, Campinas, SP 13083-970, Brazil

^e Department of Structural and Functional Biology, Institute of Biology, State University of Campinas, Campinas, São Paulo, Brazil

^f National Institute of Photonics Applied to Cell Biology (INFABiC), Campinas, São Paulo, Brazil

^g Laboratory of Exercise Physiology, School of Physical Education, University of Campinas, Campinas, SP 13083-970, Brazil

^h Laboratory of Investigation in Metabolism and Diabetes (LIMED)/Gastrocentro, Department of Surgery, University of Campinas (UNICAMP), Campinas, SP 13081-970, Brazil

ⁱ Biomedical Engineering Center, University of Campinas (UNICAMP), Campinas, SP, Brazil

^j Department of Radiology, University of Campinas, Campinas, São Paulo 13084-970, Brazil

^k Department of Pediatrics, Federal University of Uberlândia, Uberlândia, Brazil

ARTICLE INFO

Article history:

Received 14 August 2018

Received in revised form 13 November 2018

Accepted 19 November 2018

Available online 27 November 2018

One Sentence Summary: Deficiency of IL10 and systemic inflammation promote severe structural and functional damage to brown adipose tissue mitochondria.

Keywords:

Interleukin-10

Inflammation

Thermogenesis

Mitochondria

Respiration

Obesity

ABSTRACT

Background: Inflammation is the most relevant mechanism linking obesity with insulin-resistance and metabolic disease. It impacts the structure and function of tissues and organs involved in metabolism, such as the liver, pancreatic islets and the hypothalamus. Brown adipose tissue has emerged as an important component of whole body energy homeostasis, controlling caloric expenditure through the regulation of non-shivering thermogenesis. However, little is known about the impact of systemic inflammation on the structure and function of brown adipose tissue.

Methods: The relations between IL10 and mitochondria structure/function and also with thermogenesis were evaluated by bioinformatics using human and rodent data. Real-time PCR, immunoblot, fluorescence and transmission electron microscopy were employed to determine the effect of IL10 in the brown adipose tissue of wild type and IL10 knockout mice.

Findings: IL10 knockout mice, a model of systemic inflammation, present severe structural abnormalities of brown adipose tissue mitochondria, which are round-shaped with loss of cristae structure and increased fragmentation. IL10 deficiency leads to newborn cold intolerance and impaired UCP1-dependent brown adipose tissue mitochondrial respiration. The reduction of systemic inflammation with an anti-TNF α monoclonal antibody partially rescued the structural but not the functional abnormalities of brown adipose tissue mitochondria. Using bioinformatics analyses we show that in both humans and mice, IL10 transcripts correlate with mitochondrial lipid metabolism and caspase gene expression.

Interpretation: IL10 and systemic inflammation play a central role in the regulation of brown adipose tissue by controlling mitochondrial structure and function.

Fund: Sao Paulo Research Foundation grant 2013/07607-8.

© 2018 The Authors. Published by Elsevier B.V. This is an open access article under the CC BY-NC-ND license (<http://creativecommons.org/licenses/by-nc-nd/4.0/>).

1. Introduction

Brown adipose tissue (BAT) is regarded as a potential target for approaches aimed at treating obesity and some of its comorbidities, particularly type 2 diabetes (T2D) [39,59,65]. Upon stimulation by cold or β -adrenergic drugs, for example, the mitochondria-rich BAT increases the uptake of distinct substrates, which are employed to

* Corresponding author at: Laboratory of Cell Signaling, Department of Internal Medicine, University of Campinas, Campinas, São Paulo 13084-970, Brazil.

E-mail address: lavelloso@fcm.unicamp.br (L.A. Velloso).

¹ The Laboratory of Cell Signaling belongs to the National Institute of Science and Technology – Neuroimmunomodulation (INCT-NIM).

conduct thermogenesis by either uncoupling protein-1 (UCP1) - dependent uncoupled respiration [40,50] or by ATP-linked mechanisms, such as creatine-dependent thermogenesis or lipid futile cycling [33,60], thus increasing whole body energy expenditure. Employing [¹⁸F]-fluorodeoxyglucose (FDG) uptake as determined by positron emission tomography combined with X-ray computed tomography (FDG-PET/CT), studies have identified a number of factors that are physiologically related to increased BAT activity, such as cold-exposure, leanness, youth, physical activity and the female gender [13,67,72]. Conversely, in pathological conditions such as obesity and T2D not only is baseline BAT glucose uptake low, but the capacity of inducing its activity by different approaches is impaired [48,54].

Currently, there are 50 ongoing clinical trials aimed at developing new strategies to stimulate BAT activity in obesity (Suppl. Table 1). Among the studies evaluating drugs that are expected to increase BAT activity, there are β -adrenergic, GLP1, PPAR γ and thyroid hormone agonists. Surprisingly, none of the clinical trials aim to dampen inflammation as an approach to stimulate BAT.

Here, we tested the hypothesis that systemic inflammation could impair BAT activity. This hypothesis was tested using distinct approaches and models. Interleukin-10 (IL10) knockout mice (IL10 KO) were employed as a model of systemic inflammation. These mice present a deregulated control of interferon-gamma (IFN γ) producing CD4-T lymphocytes leading to exacerbated Th1 activity [53]. We also evaluated markers of thermogenesis in two patients with mutation of the IL10 receptor (IL10RA); these patients present chronic systemic inflammation. In addition, we used bioinformatics to analyze large human and rodent public dataset asking if IL10 was correlated with markers of mitochondria function and structure and also with markers of thermogenesis.

2. Results

2.1. IL10 is associated with BAT function and oxygen consumption in humans

In order to explore the hypothesis that systemic IL10 levels correlate with BAT function, we employed transcriptome-based bioinformatics analysis to examine the correlation between IL10 and blood transcripts using a human dataset that included 175 subjects [12]. IL10 correlated positively with mitochondrial and lipid metabolism genes (Fig. 1A), as well as genes involved in mitochondrial dynamics (Fig. 1B–C). In adipose tissue, IL10 transcripts correlated positively with mitochondria, lipid metabolism and caspase pathway related transcripts (Fig. 1D). Adipose tissue IL10 also correlated with some mitochondrial dynamics genes, particularly Opa1 and Mfn2 (Fig. 1E–F). Next, we evaluated a group of subjects with metabolically controlled T2D (Suppl. Table 2). Blood IL10 was not correlated with BAT volume (Fig. 1G); however, it was directly correlated with standardized uptake value (SUV) (Fig. 1H–J). In addition, there was neither correlation with basal metabolic rate (Fig. 1K) nor with non-shivering thermogenesis (Fig. 1L). In another cohort of obese, non-diabetic subjects submitted to bariatric surgery (Suppl. Fig. 1 and Suppl. Table 3), BAT volume was increased (Suppl. Fig. 2A), whereas SUV was not modified following body mass reduction eight months after surgery (Suppl. Fig. 2B–D). Blood IL10 was not modified (Suppl. Fig. 2E), whereas energy expenditure (Suppl. Fig. 2F) and respiratory quotient (Suppl. Fig. 2G) reduced and glucose infusion rate during a hyperinsulinemic-euglycemic clamp increased (Suppl. Fig. 2H). Both before and after surgery there were direct correlations between IL10 and basal metabolic rate (Suppl. Fig. 2I and K), whereas no correlation was found for IL10 and SUV (Suppl. Fig. 2J and L).

2.2. IL10 correlates with BAT metabolism and mitochondria related transcripts in mice

Next, we performed bioinformatics analysis employing a dataset of BAT transcripts from distinct mice families [1]. There were direct correlations between BAT IL10 and mitochondrial-NAD replenishers, lipid metabolism and caspase/ubiquitin related transcripts (Fig. 2A). In addition, using a public gene expression dataset from C57/BL6 mice, we demonstrate that adipose tissue IL10 and STAT3 expressions were stimulated shortly after treatment with the β 3-adrenergic agonist CL-316,243 [24] (Fig. 2B). However, acute treatment of mice with IL10 increased neither BAT temperature nor O₂ consumption (Suppl. Fig. 3A–E). In addition, in an immortalized BAT adipocyte cell line, acute treatment with IL10 did not modify PKA substrate phosphorylation (Suppl. Fig. 3F–G).

2.3. Reduced whole body IL10 leads to cold intolerance

At baseline (room temperature 22 ± 1 °C), IL10 KO mice presented lower BAT temperature (Fig. 2C–D) and similar whole-body energy expenditure per lean-mass as compared with wild-type mice (Fig. 2E) and this was accompanied by reduced BAT weight (Suppl. Fig. 4A). However, BAT total protein, BAT protein density, and BAT total UCP1 and UCP1 adjusted for total BAT protein were similar to control (Suppl. Fig. 4B–E). In addition, there were no differences in CL-316,243-stimulated changes in BAT temperature and whole body O₂ consumption (Suppl. Fig. 4F–G). Upon cold exposure (4 °C), adult IL10 KO mice presented 50% mortality after 6 h (Fig. 2F). This was not accompanied by changes in BAT or tail temperature (Fig. 2G–H). In newborn wild-type C57/BL6 mice, the immunoneutralization of IL10 resulted in 100% mortality after 5 h of cold-exposure (Fig. 2I), which was accompanied by reduced BAT and tail temperatures (Fig. 2J–K). In order to determine if IL10 deficiency could affect diet-induced thermogenesis, we fed mice on a high-fat diet for four weeks and evaluated parameters related to energy-expenditure; as shown in Suppl. Fig. 5A–B, the consumption of a high-fat diet promoted similar changes in O₂ consumption in WT and IL10 KO mice. In addition, there were no genotype differences in BAT Pgc1 and Ucp1 transcripts (Suppl. Fig. 5C–D) either in mice fed chow or a high-fat diet.

2.4. Impaired baseline and UCP1-dependent BAT mitochondrial respiration in IL10 KO mice

In order to determine in vivo thermogenic responses, mice were exposed to cold (4 °C) for 2 h and then submitted to a PET/CT scan. There was no difference in [¹⁸F]-FDG uptake by BAT between WT and IL10 KO mice (Suppl. Fig. 6A–B). In addition, using in vivo three-dimensional multiphoton image stacks, we showed that mean lifetime of FAD and NADH were longer in IL10 KO BAT, which resulted in no difference in the redox potential of NADH (Suppl. Fig. 6C–E). In order to further explore the potential impact of IL10 deficiency on mitochondrial function in BAT, we determined oxygen consumption in isolated mitochondria. As shown in Fig. 3A–B, complex I-driven respiration (pyruvate + malate), under state 2 as well as under state 3u, and UCP1-dependent respiration (Fig. 3A–B) were impaired in IL10 KO mice. Conversely, there were no changes in phosphorylative respiration, either coupled to maximal ATP synthesis (state 3_{ADP}) or after inhibition of ATP synthase (state 4_{oligo}). The expression of TFAM and OXPHOS complex proteins were similar between IL10 KO and wild-type mice (Suppl. Fig. 7A–D). Respiration was not affected in mitochondria isolated from the liver of IL10 KO mice (Suppl. Fig. 7E). Because IL10 KO mice present a baseline inflammatory phenotype with elevated blood TNF α [18], which could potentially affect BAT mitochondria function, we treated mice for two weeks with an anti-TNF α monoclonal antibody (Infliximab) and evaluated mitochondrial function. As depicted in Fig. 3C, the immunoneutralization of TNF α did not modify basal,

maximal or UCP1-dependent mitochondrial respiration in IL10 KO mice. Together, these data show that IL10 KO mice present reduced UCP1-dependent and maximal respiratory capacity in BAT mitochondria that is not modified by the inhibition of TNF α .

2.5. Changes in transcript expression of mitochondrial genes in rodent and human IL10 related genetic defects

A transcriptome analysis (RNAseq) was performed using samples obtained from BAT of IL10 KO and respective control mice (Fig. 3D–G). As shown in Fig. 3D, there was a major impact of IL10 deficiency on the whole transcriptome of mice BAT. In functional cluster analysis, organelle membrane and mitochondria inner membrane transcripts were among the most important groups of BAT genes undergoing differential regulation related to IL10 deficiency (Fig. 3E–G). In order to provide a clinical proof-of-concept for the experimental evidence of IL10/inflammation-dependent abnormalities of BAT mitochondria, we performed a whole-blood transcriptome analysis using two female siblings that were homozygous for a synonymous mutation located at the last base pair of exon 4 of the IL10RA gene (homozygous: c537G > A: p.T197 T splicing). This pathogenic mutation (9) alters the splice donor site, resulting in two different mRNA splice products: i, an 18 bp deletion of the 3' end of exon 4; ii, a product lacking exon 4 (170 bp). The girls had a genetic diagnosis made early in life because of a severe intestinal inflammatory condition diagnosed as Crohn's disease. The parents were also evaluated as controls. Similar to the finding in BAT of IL10 KO mice, IL10 signaling defect in humans was accompanied by a major change in blood transcript expression (Fig. 3H). Mitochondrial outer membrane transcripts were among the most significantly changed cluster of genes modified by the IL10RA defect (Fig. 3I–K). A number of mitochondria dynamics related transcripts were similarly regulated in BAT of IL10 KO mice and blood of humans with mutation of the IL10RA gene (Fig. 3L).

2.6. IL10 KO mice have abnormal mitochondrial structural organization and dynamics shifted toward fission

Analysis of mitochondria ultrastructure under transmission electron microscopy showed that BAT mitochondria of IL10 KO mice presented an aberrant structure with a round shape and complete disorganization of cristae (Fig. 4A). This was not observed in skeletal muscle, which presented mitochondria with normal shape and cristae in IL10 KO mice (not shown). Again, because of the potential involvement of systemic inflammation in the abnormalities of BAT mitochondria in IL10 KO mice, we treated mice with Infliximab and evaluated BAT mitochondria morphology; in this case, despite the fact that most mitochondria remained with a round shape, cristae organization was mostly corrected (Fig. 4A). Counting under transmission electron microscopy determined there were no changes in mitochondrial number (Fig. 4B); however there were reductions of total cristae length per mitochondria (Fig. 4C), reductions of cristae number per mitochondria (Fig. 4D), reductions of ratio between longest and shortest mitochondria axis (Fig. 4E) and no changes in mitochondria circularity (Fig. 4F). All these mitochondrial defects were at least partially rescued by the inhibition of TNF α (Fig. 4C–F). Since IL10 loss was accompanied by an apparent fragmentation of BAT mitochondria, we evaluated the effects of immunoneutralization of IL10 on OPA1, which is a protein involved in cristae ultrastructure integrity; as shown in Fig. 4G–I there were no changes in the total protein amounts of MFN2 or the long or short form of OPA1. To further explore the role of IL10 in the regulation of proteins involved in BAT mitochondrial dynamics, we acutely treated an immortalized BAT adipocyte cell line with either IL10 or an immunoneutralizing IL10 antibody; as shown in Fig. 4J–K, IL10 immunoneutralization resulted in no change in the proportion of the fusion-deficient short form of OPA1. Finally, MEFs expressing dsRed-Mito were treated with either an immunoneutralizing IL10 antibody

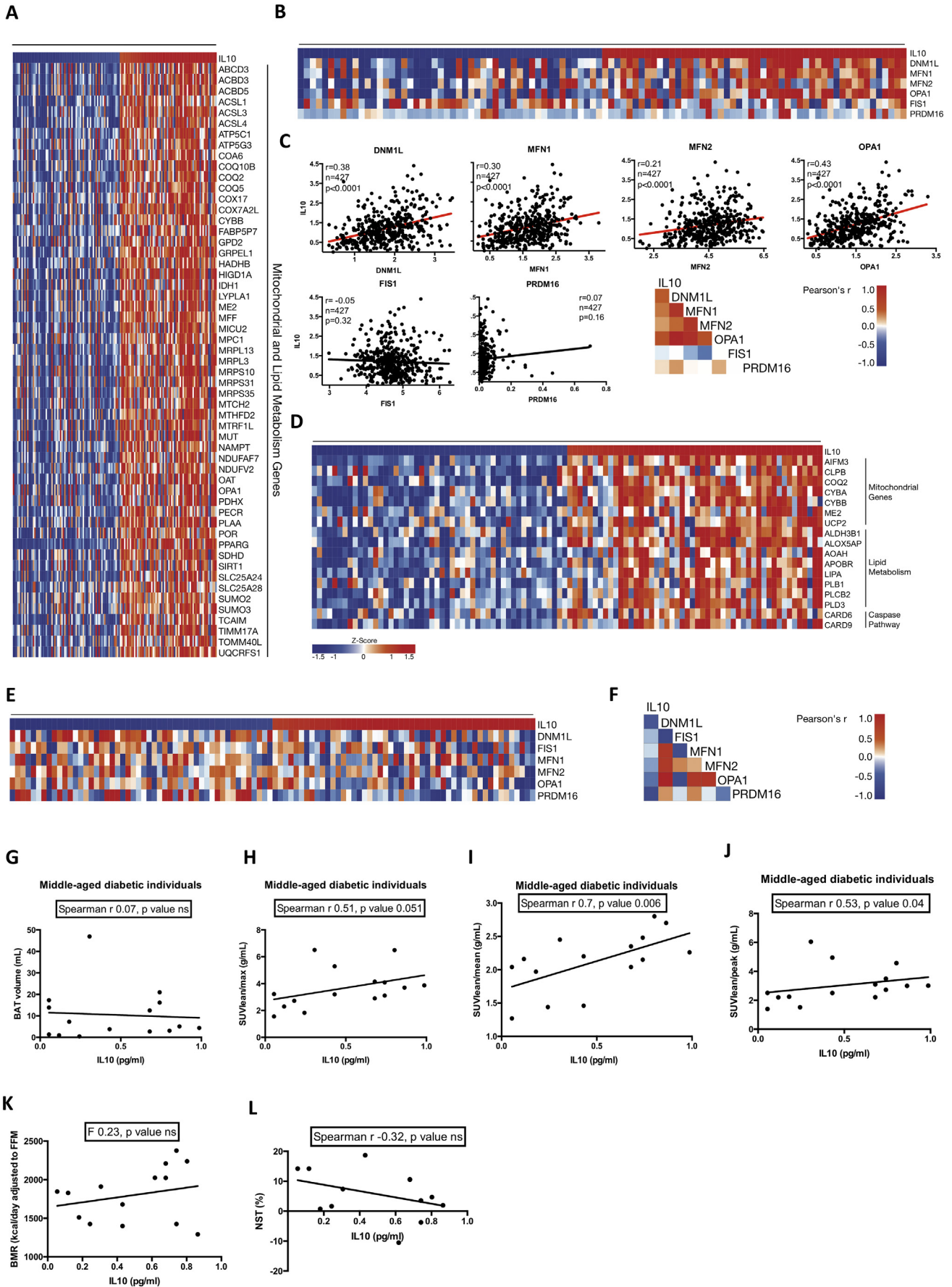
or rotenone and the mitochondrial network was evaluated; as show in Fig. 4L–Q, the immunoneutralization of IL10 led to increased mitochondria fragmentation (Fig. 4L–O) and reductions in the aspect ratio (Fig. 4P) and the form factor (degree of branching) (Fig. 4Q).

3. Discussion

Systemic low-grade inflammation is a hallmark of obesity and is regarded as the most important mechanism linking obesity and insulin resistance [28,68]. Studies have provided strong experimental and clinical evidence to support a role for inflammation in the dysfunction of most tissues/organs with important involvement in metabolism, which are structurally and functionally affected during the course of obesity [27]. This can be exemplified and illustrated by changes in structure (steatosis/fibrosis/cirrhosis) and function (abnormal lipid and glucose metabolism) in the liver [6,41], as well as changes in structure (gliosis/loss of blood-brain barrier integrity) and function (abnormal control of food intake) in the hypothalamus in obesity [9,31,49]. BAT has emerged as a promising target for the treatment of obesity because of its involvement in thermal regulation of endothermic organisms, producing heat at the expense of energy [56]. However, the role of inflammation in the putative structural and functional abnormalities of BAT in obesity is still a matter of investigation.

Here, we employed an animal model of chronic systemic inflammation to evaluate potential changes in BAT structure and function. IL10 KO mice are widely used in studies aimed at evaluating the impact of inflammation on distinct organs and systems [44,53]. They present increased circulating levels of inflammatory cytokines and abnormal regulation of both innate and adaptive immune responses [52,53]. The potential involvement of anomalous systemic immune regulation caused by abnormalities in the IL10 system in insulin resistance and obesity has been previously evaluated in experimental and clinical/epidemiological studies [11,66]. In humans, this was convincingly shown by the demonstration that a decreased capacity to produce IL10 is associated with insulin resistance and metabolic syndrome [66]. In rodents, the beneficial effects of IL10 to protect against insulin resistance has been demonstrated by different approaches that, taken together, suggest IL10 can act directly to improve insulin action, and indirectly by controlling inflammation and, consequently, attenuating insulin resistance [11,26,34,45].

Before evaluating the structural and functional aspects of BAT in IL10 KO mice, we used bioinformatics to evaluate whether IL10 transcript levels would correlate with the transcripts of proteins intimately related to BAT function and/or thermogenic activity. For that, we took advantage of large public transcript databases that have been previously used to study other metabolic questions ([1]; Schughart and consortium, 2010). In both humans and mice, we found direct correlation of IL10 with mitochondrial function, mitochondrial dynamics and lipid metabolism, which strongly supported our working hypothesis. This was further supported by the transcriptome analysis of IL10 KO mice BAT, which displayed a similar spectrum of abnormalities to the one detected in the whole blood transcriptome analysis of two girls with a mutation of the IL10RA gene. In order to seek further clinical support for our hypothesis, we evaluated two cohorts of obese patients. One cohort was evaluated in cross-section analysis and the other was evaluated before and after undergoing bariatric surgery. Obesity is one of the main factors contributing to low BAT glucose uptake in humans [23,48,70,71]. Upon reduction of body mass, BAT glucose uptake increases in association with both the attenuation of insulin resistance and reduction of systemic inflammation [48,54,70]. It is currently unknown if the changes in BAT glucose uptake detected in obese and diabetic subjects reflect a functional abnormality of the tissue or simply a change in metabolism with preferential use of fatty acids, instead of glucose in order to maintain thermogenic activity, as previously suggested [7]. Nevertheless, here, we showed that in the cohort evaluated at baseline and in the cohort evaluated before surgery there was a correlation



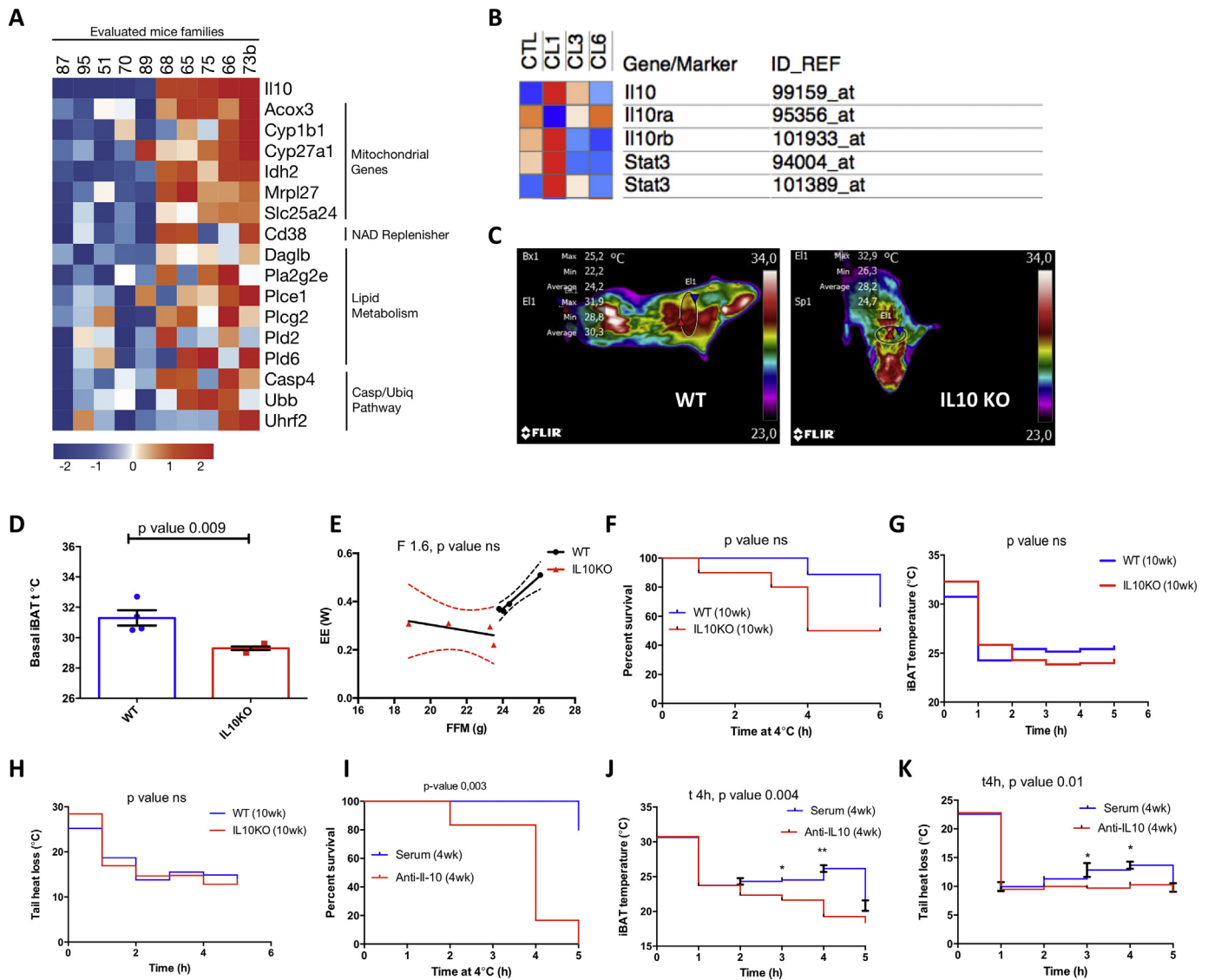


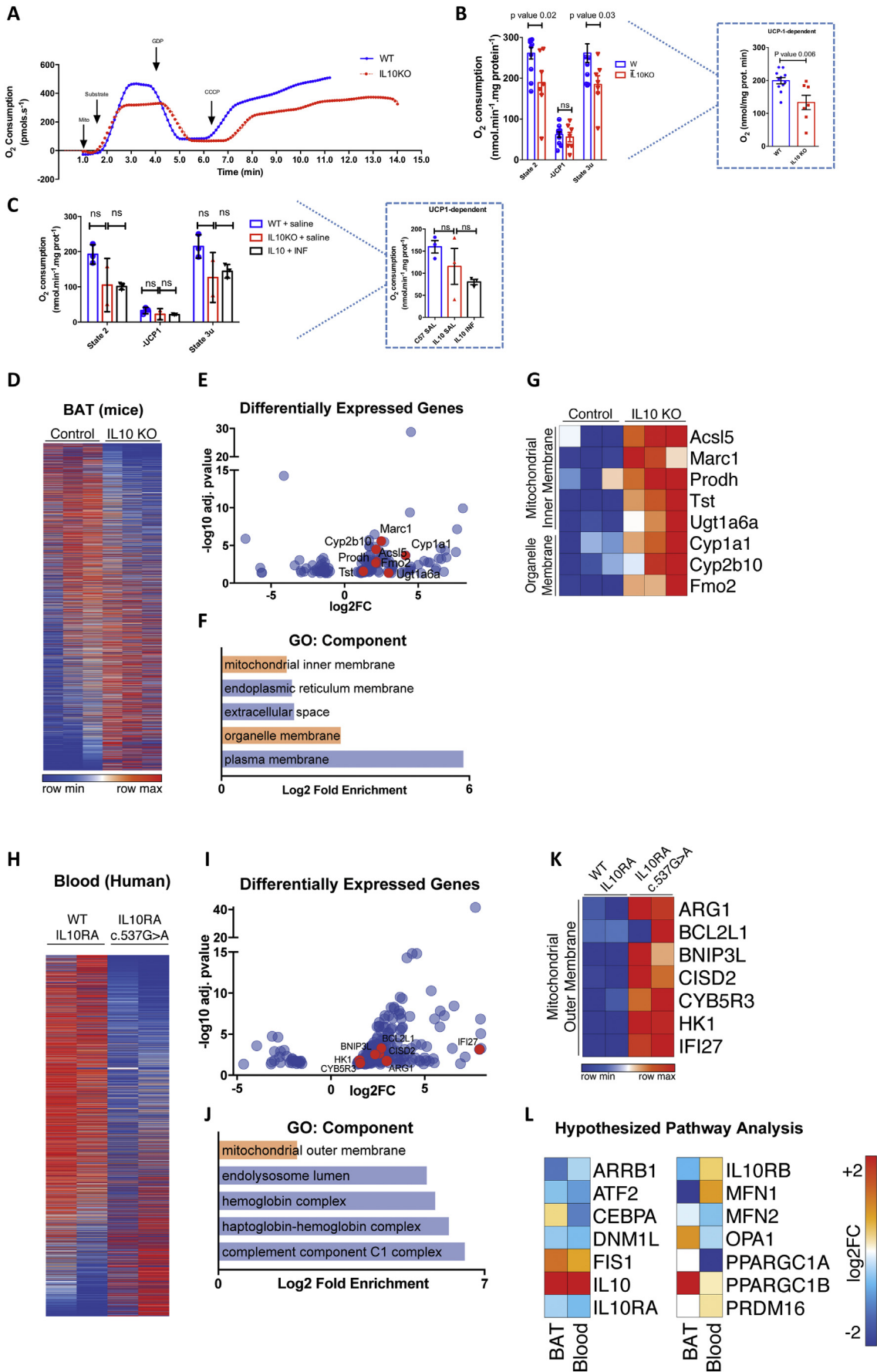
Fig. 2. IL10 deficiency promotes cold intolerance in mice. A, Heatmap of correlation between IL10 transcripts and mitochondrial, NAD replenisher, lipid metabolism and caspase/ubiquitin pathways related transcripts in brown adipose tissue of mice. B, Heatmap of the expression levels of IL10, IL10ra, IL10rb and Stat3 in the subcutaneous adipose tissue of mice after short-term treatment with a beta 3-adrenergic agonist CL-316,243 during 1, 3 or 6 days (CL1–CL6); CTL, control. C–D, Basal surface infrared thermography analysis of iBAT temperature in wild-type (WT) and IL10KO mice housed at 22 °C. E, Energy expenditure (EE) per animal is plotted against lean body mass (measured by dual energy X-ray absorptiometry). F, Percent survival of 10-week-old male mice challenged with cold ($n = 6$ per genotype). G–H, Infrared thermography analysis; surface iBAT temperature of 10-week-old male mice challenged with cold (G); and tail temperatures obtained 0.5 cm from the tail base (H). I, Percent survival of 4-week-old male mice treated during 2 weeks with serum (40 ng per mouse) or anti-IL10 antibody (40 ng per mouse) challenged with cold ($n = 6$). J–K, Infrared thermography analysis; surface iBAT temperature of 4-week-old male mice treated during 2 weeks with serum (40 ng per mouse) or anti-IL10 (40 ng per mouse) challenged with cold, and tail temperatures obtained 0.5 cm from the tail base from 4-week-old male mice treated during 2 weeks with serum (40 ng per mouse) or anti-IL10 (40 ng per mouse) challenged with cold.

between IL10 and BAT activity, as measured by glucose uptake; whereas after body mass reduction this association was lost. This finding further suggests that both IL10 and systemic inflammation play combined roles in the control of BAT in humans.

In IL10 KO mice, the most remarkable finding was that virtually all mitochondria visualized under transmission electron microscopy

presented a round shape with severe damage of the cristae. This aspect suggests mitochondrial swelling, which is an abnormality known to occur in conditions such as cancer [3], chronic liver disease [25], exposure to certain pharmacological agents [14] and poisoning [46]; and, the causes could be changes in transition permeability [51] and Ca^{2+} overload [22]. Mitochondrial volume

Fig. 1. IL10 is associated with mitochondrial genes and energy expenditure. A, Heatmap of the correlation between whole-blood IL10 mRNA levels and mitochondrial/lipid metabolism genes and IL10 mRNA in whole-blood; in the right-hand bottom corner of C, the same data is expressed using a corrgram showing the positive (red) and negative (blue) correlations between whole-blood IL10 mRNA and mitochondrial dynamic-related genes. D, Heatmap of the correlation between mitochondrial, lipid and caspase genes and IL10 mRNA levels in adipose tissue. E, Heatmap of the correlation between IL10 mRNA and mitochondrial dynamics-related genes in adipose tissue. F, Corrgram showing the positive (red) and negative (blue) correlations between IL10 mRNA and mitochondrial dynamics-related genes in adipose tissue. In G–L, correlation plots of serum IL10 levels and brown adipose tissue (BAT) volume (G), standardized uptake value (SUV) lean/maximal (H), SUV lean/mean (I), SUV lean/peak (J), basal metabolic rate (BMR) (K), and non-shivering thermogenesis (NST) (L). In A–F, data of 175 healthy humans was obtained from a public database [12]; in G–L, data was from 15 middle-aged patients with type 2 diabetes.



homeostasis is essential for preserving the structural integrity of the organelle, and depending on the magnitude and persistence of stimuli leading to this alteration, it can be accompanied by changes in mitochondrial function [32].

We performed a number of experiments to evaluate different aspects of BAT mitochondrial function in IL10 KO mice. First, we demonstrated that genetic disruption of IL10 resulted in lower BAT temperature when mice were maintained at room temperature and reduced thermogenic capacity when mice were exposed to cold. This phenotype was, to a certain degree, similar to the one described for UCP1 deficient mice [19]. Despite the fact that UCP1 expression was not affected, BAT mitochondria from IL10 KO mice presented defects in baseline and UCP1-dependent respiration. Abnormal mitochondrial cristae structure and defective respiration associated with thermogenic instability have been reported in mice lacking components of the mitochondria fusion/fission machinery, particularly affecting OPA1 [47]. Despite the fact that OPA1 protein levels were not altered in IL10 KO mice, human bioinformatics analysis showed that the expression of IL10 in adipose tissue was correlated with OPA1, further suggesting that the IL10 system controls, either directly or indirectly, mitochondrial dynamics.

OPA1 is a GTPase that plays an important role in the control of mtDNA stability, mitochondrial fusion and cristae integrity [5,69]. It has been shown that the balance between short and long forms of OPA1 is essential for the coordinated maintenance of both structure and function of mitochondria [16]. The complete deletion of OPA1 leads to severe functional and structural abnormalities of mitochondria, and the expression of either long or short isoforms can rescue the energetic defect independent of the structural abnormality [16,73]. However, in order to obtain a completely normal mitochondrial phenotype, both at the structural and functional levels, balance between short and long forms must be achieved [16]. However, it is currently unknown to what degree inflammation and abnormal IL10 function can impact OPA1.

In the context of our experimental model, we asked if the structural and functional abnormalities of BAT mitochondria were due to the lack of IL10 activity, systemic inflammation or a combination of both. For that, we employed three distinct strategies; i, immunoneutralization of TNF α using a monoclonal antibody (Infliximab) that is approved for clinical use in inflammatory diseases, such as rheumatoid arthritis and Crohn's disease [61,64]; ii, treatment of mice and cells with exogenous IL10; and iii, immunoneutralization of IL10 in wild-type mice and cells. As a whole, our experiments showed that the immunoneutralization of TNF α had a significant effect on BAT mitochondrial morphology, partially rescuing the cristae defect phenotype; however, it resulted in no change in mitochondrial respiration. Immunoneutralization of IL10 resulted in thermogenic instability, and mitochondrial fragmentation. The thermogenic instability was particularly evident in newborn mice suggesting that in adult life other mechanisms operate to protect against hypothermia in the absence of IL10. It is noteworthy that in cell culture experiments using MEF, which are mice embryonic fibroblasts, the immunoneutralization of IL10 was capable of recapitulating some of the findings in BAT of IL10 KO mice, suggesting that the mitochondria protective effect provided by IL10, is not restricted to brown adipocytes and, at least in part, can occur in cells with a low degree of differentiation. However, the treatment with

IL10 alone was not capable of changing either the function or the structure of mitochondria. Taken together, these findings reinforce the role of combined actions of IL10 and inflammation in the development of BAT mitochondrial abnormalities.

In summary, this study shows that BAT mitochondria are severely damaged at the structural and functional levels in IL10 deficiency. Both IL10 deficiency, per se, and systemic inflammation, which originated as a result of the immune imbalance resulting from the lack of IL10, act in combination to damage mitochondria. We propose that abnormal activity of the IL10 system may contribute to defects in energy metabolism in medical conditions in which systemic inflammation is present.

4. Materials and methods

4.1. Overview of the experimental procedure with humans

Subjects ($n = 41$) (Supplementary Fig. 1) were recruited at the University of Campinas Clinics Hospital (Ethics Committee approval #CAAE: 31865314.2.0000.5404) and underwent screening to evaluate eligibility. Subjects were then submitted to nutritional evaluation, body composition, and psychological evaluation. Once included, subjects were submitted to (18F)-FDG-PET/CT-scan, hyperinsulinemic-euglycemic clamp, indirect calorimetry and blood collection. Roux-en-Y Gastric Bypass (RYGB) was performed by the same surgeon (JCP) always, according to a method previously described [15]. An open-field biopsy was performed during the RYGB in the supraclavicular region in order to obtain a sample of adipose tissue located below the superficial cervical fascia. One year after RYGB, the patients were submitted to new cervical biopsy in the same site. The middle-aged diabetic subjects ($n = 16$) were also recruited at the University of Campinas Clinics Hospital (Ethics Committee approval #CAAE: 55952516.6.0000.5404) and underwent screening to evaluate eligibility. Once included, subjects were submitted to (18F)-FDG-PET/CT-scan, indirect calorimetry and blood collection.

4.2. Cold exposure protocol

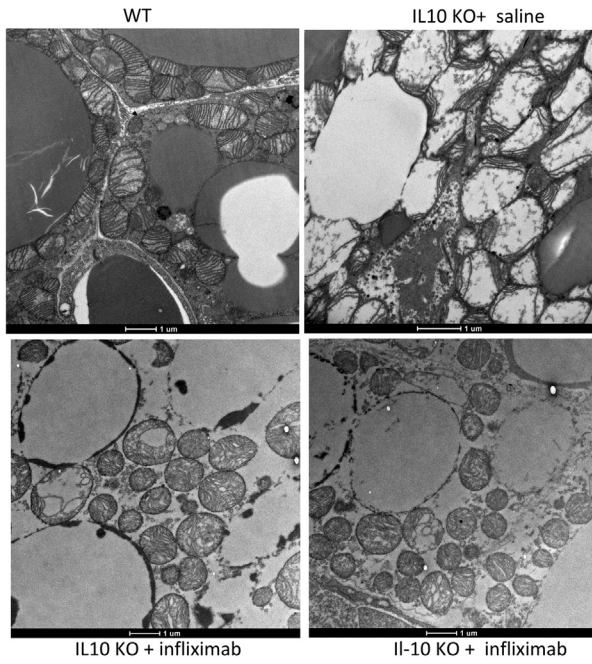
Patients and controls were admitted to a preparatory exam room wearing light clothing (0.49 clo) and exposed to 19 °C until shivering occurred. When presenting clinically detectable shivering, the room temperature was stepwise increased by 1 °C until shivering ceased, up to 22 °C. During the cold exposure, subjects were instructed to refrain from talking or performing any physical activity.

4.3. PET/CT scanning protocol

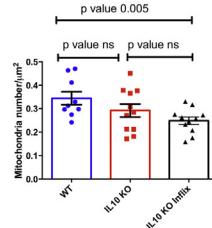
Images were acquired and processed using a Siemens PET/CT Biograph mCT 40 (Siemens Medical Solutions, Chicago, IL) and Syngo Multimodality VB10B WinNT 4.0 station, also from Siemens. An intravenous injection of 4.0 MBq/kg of (18F)-FDG was given and the patients remained in the preparatory exam room for an additional 1-h before images were acquired. (18F)-FDG was obtained from the Nuclear and Energy Research Institute (IPEN, Sao Paulo, Brazil). The CT part of the PET/CT study was performed as a low-dose acquisition with 130 kV,

Fig. 3. IL10 deficiency promotes impaired UCP1-dependent respiration and changes in transcript expression of mitochondrial genes. A, Mitochondrial respiration traces obtained from assays performed with brown adipose tissue isolated mitochondria from wild-type (WT) and IL10 KO mice. B, Quantification of complex I-driven (in the presence of 5 mM pyruvate plus 3 mM malate) oxygen consumption rates (OCR) in brown-fat isolated mitochondria from wild type (WT) and IL10 KO mice under different respiratory states; UCP1-dependent respiration is depicted in the inset. C, Quantification of complex I-driven (pyruvate-malate) oxygen consumption rates (OCR) in brown-fat isolated mitochondria from wild type (WT) and IL10 KO mice treated with saline or infliximab during 2 weeks under different respiratory states; UCP1-dependent respiration is depicted in the inset. D, Brown adipose tissue (BAT) expression profile of control and IL10 KO mice. E, Volcano plot of differentially expressed genes (DEGs), adjusted p -values < .05. F, Gene Ontology analysis showing some of the enriched components from DEGs. G, Heatmap showing DEGs from mitochondrial inner membrane and organelle membrane. H, Human blood serum expression profile from samples of control (WT) and patients with mutation of IL10RA. I, Volcano plot of DEGs, adjusted p -values < .05. J, Gene Ontology analysis showing some of the enriched components from DEGs. K, Heatmap showing DEGs from mitochondrial outer membrane. L, Heatmap showing log₂ fold change of genes involved in thermogenesis according to the literature and suggested mechanisms involving IL10 and heat production from BAT and blood samples (versus respective controls). Bar graphs show average \pm SEM per experiment ($n = 3$ - pool of 3 mice per group).

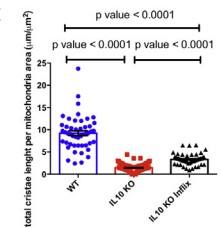
A



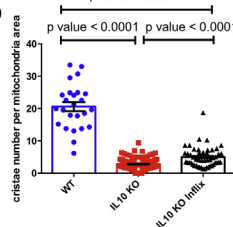
B



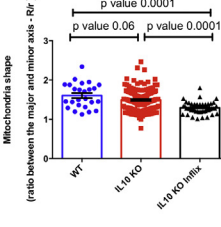
C



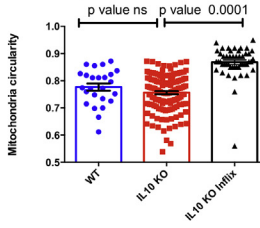
D



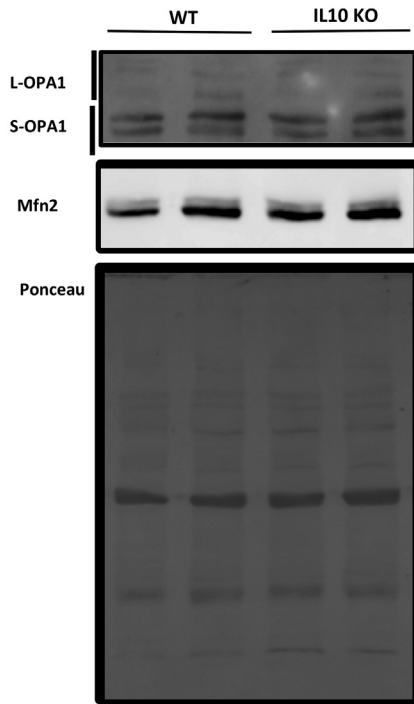
E



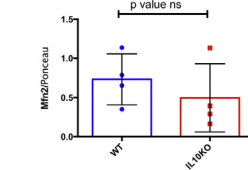
F



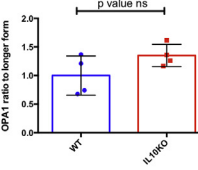
G



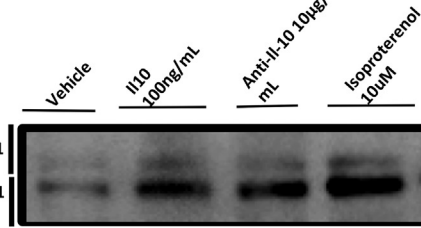
H



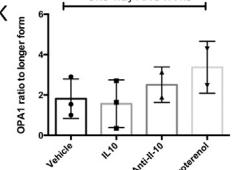
I



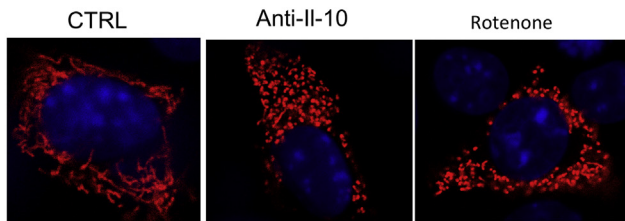
J



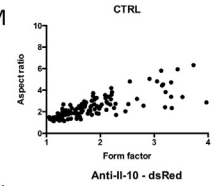
K



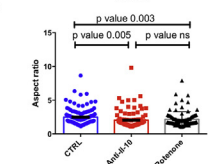
L



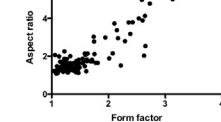
M



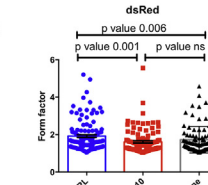
P



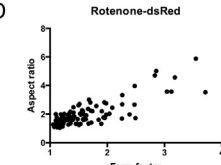
N



Q



O



50–80 mA, 0.8 s per CT rotation, pitch 4.0–5.0 mm, field of view of 500 mm and a scan speed of 24.6 mm/s. The PET scan was performed immediately after the CT scan without changing the position of the patient, always in the craniocaudal direction from head to proximal thighs. Images were acquired in five to seven bed positions, 4.0 min/bed position. The voxel size of reconstructed PET and CT image sets were $2.500 \times 2.500 \times 5.000$ mm³ and $0.977 \times 0.977 \times 5.000$ mm³, respectively.

4.4. PET/CT image analyses

The scans were analyzed using Fiji software and the PET/CT Viewer Plug-in following the instruction on petctviewer.org. The free PET/CT plug-in was developed for BAT evaluation by Beth Israel Deaconess Medical Center [37]. Three researchers (JCLJ, BJA and CDR) evaluated the PET/CT images independently; BJA and CDR are experienced nuclear medicine physicians. The PET images with a resolution of 5-mm were imported into ImageJ for image processing, along with low-dose CT images. Specific CT and PET ranges were set up to localize fat (−300 to −10 HU) and active brown fat (SUV lean(g/mL) > 1.2). For BAT SUV normalized to LBM, the activity was measured using $SUV_{lean} = 1.2 \text{ g/mL}$ corrected for BOD-POD-measured LBM (in middle-aged diabetic sample) [37] or using sex-specific Janmahasatian formulation, which is expected to be accurate for very obese subjects (in RYGB individuals) [63]. We draw one ROI on each axial slice according to 3D-axial method, avoiding overlapping or false-positive depots, from C3 vertebra-to-vertebra T3 identifying cervical and supraclavicular depots [42]. Next, we draw new segmented (cervical and supraclavicular) ROIs only in the BAT mask containing voxels confirmed as BAT [37]. We used BARCIST 1.0 criteria to define $SUV_{lean}/mean$, SUV_{lean}/max , $SUV_{lean}/peak$ and BAT volume [10].

4.5. Indirect calorimetry in humans

Indirect calorimetry was performed using a Vmax (Yorba Linda, CA, USA) automated gas analysis system. After an equilibration period of 10 min, the average gas exchange rates recorded over two 30 min steady-state periods (90–120) were used to calculate rates of glucose oxidation, lipid oxidation and respiratory exchange ratio (RER) and resting energy expenditure (REE) as previously described [21].

4.6. Body composition

Fat mass (FM) and fat-free mass (FFM) were measured using air-displacement plethysmography (Bod Pod) [17]. Lean body mass (LBM) was measured using sex-specific Janmahasatian formulation [63].

4.7. Bioinformatics analysis

Correlation analyses were performed from data on BAT and phenotypes (BXD Published Phenotypes) from families of BXD inbred mice as previously published [1], as well as data on adipose tissue mRNA of human individuals (GTExv5 Human adipose tissue RefSeq (Sep15) RPKM log₂) or whole-blood mRNA of human individuals (INIA whole blood Affy MoGene 1.0 ST (Nov10)), generated as part of the

Genotype-Tissue Expression (GTEx) project (www.genenetwork.org) [12]. All are accessible on GeneNetwork. Heatmaps were created using GENE-E (The Broad Institute, www.broadinstitute.org/cancer/software/GENE-E/).

4.8. RNA sequencing (RNAseq)

Libraries were prepared using TruSeq Stranded mRNA Library Prep Kit (Illumina). Sequencing was performed at the Life Sciences Core Facility, University of Campinas, using the HiSeq. 2500 (Illumina), which resulted in ~20 million reads per sample. Reads were analyzed for quality, filtered and trimmed using FASTQC, available at: <https://www.bioinformatics.babraham.ac.uk/projects/fastqc/> [2] and Trimmomatic [8]. Reads were aligned using Bowtie2 software for human and mouse genomes [36]. Differentially expressed genes (DEGs) were identified using RSEM software [38]. Gene Ontology analysis was performed using DAVID 6.8 Beta [29]. Heatmaps were created using GENE-E software (<http://www.broadinstitute.org/cancer/software/GENE-E/index.html>).

4.9. Mice

C57/BL6 mice were obtained from Experimental Animal Facility, University of Campinas. B6.129P2-IL10tm1Cgn/J mice, IL10 KO, were obtained from Experimental Animal Facility, University of São Paulo, and were originally imported from Jackson Laboratories. The mice were fed and acclimated according to the regulations of the Institutional Animal Care and Use Committee (IACUC). In the study, only 8–12 week male mice acclimatized at 22 °C were used in a light cycle of 12 h and a dark cycle of 12 h with free access to water and food. All animal procedures were approved by the University of Campinas Ethics Committee. Animals were sacrificed by cervical dislocation after intraperitoneal anesthesia with xylazine (10 mg/kg) and ketamine (120 mg/kg) to obtain interscapular BAT.

4.10. Reagents and antibodies

The following reagents were used: oligomycin, FCCP, rotenone, antimycin A, ADP, GDP, isoproterenol, CL 316,243 (Tocris Bioscience), isobutylmethylxanthine, dexamethasone, insulin, rosiglitazone, T3, recombinant mouse IL10 (Calbiochem, Cat# 407700), RNeasy (Qiagen), Lipofectamine 3000 (Life Technologies). DNA vectors: pDsRed2-Mito Vector (Clontech). Antibodies as follows: anti-UCP-1 (Abcam, ab10983), anti- Phospho-(Ser/Thr) PKA Substrate (Cell Signaling #9621), anti-OPA1 (Abcam, ab42364), anti-mitofusin-2 (Abcam, ab 50843), anti-alpha-tubulin (Abcam, ab4074), anti- mtTFA ((A-17): sc-23588), anti-IL10 (Santa Cruz, sc-8438) and anti-OXPHOS cocktail (Abcam, ab110413).

4.11. Cell culture

Brown immortalized preadipocytes were developed as previously described [43]. The preadipocytes were differentiated after grown adipocytes to 95–97% confluence in complete medium following standard protocol (DMEM containing 10% FBS, 0.5 mM isobutylmethylxanthine, 1 mM dexamethasone, 20 nM insulin, rosiglitazone 0.5 μM and

Fig. 4. IL10 deficiency impairs ultrastructural mitochondria organization and shifts dynamics toward fission. A, Transmission electron microscopy (TEM) imaging of brown adipose tissue of wild-type (WT) and IL10 knockout mice treated with saline or infliximab (100 μg in 100 μl saline/dose, i.p., twice a day, during two weeks). Using TEM images the following parameters were determined: mitochondrial number (B), total cristae length per mitochondria area (C), cristae number per mitochondria area (D), ratio between the major and minor axis of mitochondria (E) and mitochondria circularity (F). G, Representative Western blot measuring Opa1 and Mfn2 in total lysates from BAT-IL10-KO (KO) male mice and wild type (WT). After stripping, the membrane was used to blot against UCP1 in the Supp. Fig. 3E, TFAM and OXPHOS (Suppl. Fig. 6 A). H, determination of Mfn2 protein expression in immunoblot; I, determination of the ratio short/long forms of Opa1 (N = 5 per group). J, Representative Western blot measuring Opa1 in total lysates from immortalized brown adipocyte cell line treated with either recombinant IL10 or an immunoneutralizing IL10 antibody. K, Densitometry quantification of Opa1 short form to longer form (N = 3 per group). L, MEF expressing pDsRed2-Mito and imaged after treatment with DMSO, anti-IL10 (10 μg/mL) or rotenone (500 nM) during 12 h. M–O, Plots of aspect ratio against form factor calculated from the image L. P–Q, Means ± SEM of aspect ratio (P) and form factor (Q) obtained from the data in L quantified in (M–O). N = 70 cells in total. Statistical analysis was performed using ordinary one-way ANOVA.

1 nM T3 for 2 days, then followed by 5–7 days of incubation with DMEM containing 10% FBS, 20 nM insulin, rosiglitazone 1 μ M and 1 nM T3 [4].

4.12. IL10 pharmacological studies

Previously, male C57BL/6j mice (8–10wk) were acclimated to the metabolic chamber five days before start the experiment. Indirect calorimetry was taken for 24 h to obtain basal values before injections (last 120 min). To assess CL 316,243-induced thermogenesis and the effect of IL10 on energy expenditure, the mice were removed from the chamber and treated acutely through subcutaneous administration of saline (0.9% saline), or recombinant IL10 (10 μ g/kg/dose) or the β 3-agonist CL 316,243 (1 mg/kg). Then, the mice were returned to the chamber and we measured brown adipose tissue thermal release and O₂ consumption for another 120 min [20].

4.13. BAT mitochondria isolation

Interscapular brown adipose tissue (BAT) depots were dissected from 3 mice and placed in ice-cold medium 1 with 250 mM sucrose, 10 mM Hepes and 1 mM EGTA. Preparations from wild-type and IL10 KO mice were made and run in parallel. The brown adipose tissue was finely minced with scissors after free of white fat and homogenized in a Potter homogenizer. Throughout the isolation process, tissues were kept in ice. Mitochondria were isolated by differential centrifugation. Brown adipose tissue homogenates were centrifuged at 8500 g for 10 min at 4 °C. The resulting supernatant, containing floating fat, was discarded. The pellet was resuspended in ice-cold medium 1. The resuspended homogenate was centrifuged at 800 g for 10 min, and the resulting supernatant was centrifuged at 8500 g for 10 min. The resulting mitochondrial pellet was resuspended in ice-cold medium 2, containing 100 mM KCl, 20 mM Hepes (pH 7.2), 1 mM EDTA, 0.6% fatty-acid-free BSA and centrifuged at 8500 g for 10 min. The final mitochondrial pellets were resuspended in the same medium. The concentration of mitochondrial protein was measured using the Bradford method with BSA as a standard. Adapted from [58].

4.14. Oxygen consumption

Oxygen consumption rates were monitored using a Clark-type oxygen electrode coupled to a high-resolution Oroboros respirometry system at 37 °C [30]. Brown-fat mitochondria (0.0625 mg protein/mL) were incubated in a medium consisting of 125 mM sucrose, 20 mM Hepes (pH 7.2), 2 mM MgCl₂, 1 mM EDTA, 4 mM KP, 0.1% fatty-acid-free BSA. Respiratory activity of mitochondria was measured using 5 mM pyruvate plus 3 mM malate. UCP1-linked respiration was measured as the difference between the initial respiration rate and the residual respiration following addition of 1 mM GDP. State 4oligo was obtained after oligomycin treatment. Maximal oxygen consumption rates were obtained by addition of CCCP to a final concentration of 4 μ M–5 μ M.

4.15. In vitro cell stimulation

To stimulate brown immortalized preadipocytes, cells were incubated with DMSO, IL10 (100 ng/mL), anti-IL10 (10 μ g/mL) and isoproterenol (10 μ M) for 12 h.

4.16. Mitochondrial dynamics in MEF cells

Mouse embryonic fibroblast cells (MEFs) at density of 7×10^4 cells were plated and cultivated in DMEM medium supplemented with penicillin/streptomycin and fetal bovine serum (10%). MEF cells were transfected at 70% confluence in OPTIMEM medium using 1 μ g of the plasmid pDsRed2-Mito using Lipofectamine 3000 reagent according to the manufacturer (Life Technologies, USA). Mitochondrial morphology

was analyzed from transfected MEFs with pDsRed-Mito using at least 70 mitochondria per cell following 12 h treatment with DMSO, anti-IL10 (10 μ g/mL) or rotenone (500 nM). Aspect ratio (ratio between the major and minor axis) and form factor (degree of branching) were obtained using Fiji [55] after optimizing the contrast and applying a “top-hat” filter as previously demonstrated [35].

4.17. Protein extraction and immunoblotting

Mouse brown adipose tissue or adipocytes were prepared in RIPA lysis buffer [150 mM NaCl, 50 mM Tris, 5 mM EGTA, 1% Triton X-100, 0.5% sodium deoxycholate (DOC), 0.1% sodium dodecyl sulphate (SDS), supplemented with protease inhibitors]. The homogenate was then centrifuged at 16,100 \times g for 15 min, and the supernatant was stored at –80 °C for use. Protein concentration was determined using biuret reagent protein assay. The samples were denatured in Laemmli buffer (0.5 M Tris, 30% glycerol, 10% SDS, 0.6 M DTT, 0.012% bromophenol blue) and were heated for 5 min at 95 °C. Empirically determined quantity of protein were loaded onto the gel and were resolved by SDS-polyacrylamide gel electrophoresis (SDS-PAGE), using 4%–15% gels. Then, proteins were transferred electrophoretically to nitrocellulose membranes. Thereafter, the membranes were blocked for 1 h at room temperature in Tris-buffered saline (137 mM NaCl, 20 mM Tris-HCl, pH 7.6) containing 0.1% Tween-20 (TBS-T) and 5% low-fat milk, followed by incubation with the primary antibody overnight at 4 °C. After washing for 1 h in TBS-T with 0.5% low-fat milk, the membranes were incubated for 2 h at room temperature with the respective horseradish peroxidase (HRP)-linked secondary antibody (1:5000; GE Healthcare, Buckinghamshire, UK), prepared in TBS-T with 1% low-fat milk. For protein detection, the membranes were processed using the Clarity western ECL Substrate (ECL; BioRad), and images were acquired in Image Quant LAS4000 (GE Healthcare, Life Sciences). Additionally, after stripped the membranes were reprobated and tested for alpha-tubulin as a loading control. Image J 1.48v (National Health) or Uniscan (Lab Systems, Espoo, Finland) were used for digital quantification of band intensity.

4.18. Electron microscopy

For ultrastructural analysis of mitochondria, fragments of the adipose tissue obtained from wild type and IL10 mice were dissected, fixed with 2.5% glutaraldehyde in cacodilate buffer 0.1M (pH 7.2) and stored 2 h in the same fixative at –4 °C. The specimens were post fixed with osmium in imidazole buffer 0.2 M (pH. 7.5), and then dehydrated and embedded in Durcupan ACS (Fluka, Steinheim, Switzerland). Ultrathin cross sections were collected on formvar coated copper grids, contrasted with uranyl acetate and lead citrate, and examined in a Tecnai G2 Spirit Twin (FEI, Hillsboro, OR) transmission electron microscope operated at 80 kV. Images were acquired using a Gatan Orius SC1000B camera (Pleasanton, CA, USA). Mitochondria density, size and morphology were analyzed using ImageJ as previously described [62].

4.19. Statistical analyses

Data is expressed as mean \pm standard error of the mean (SEM). The number of subjects, mice or experimental repeats (in cell culture and isolated mitochondria experiments) is presented in respective figures. Statistical significance was calculated based on two-tailed unpaired student's *t*-test for two-group comparisons. Two-way ANOVA was used for multiple-group comparisons (Sidak's multiple comparison test). Kendall rank correlation was used for non-parametric human data. Analysis of covariance (ANCOVA) was used for comparison of energy expenditure/lean mass in mice and for determination of correlation between IL10 and basal metabolic rate in humans. A *P*-value < .05 was considered significant in the study. The sample size of mice and cells experiments were settled based on our experience. The sample

size of human protocol was determined based on previous results from our group and also by a statistical power of 0.8. We excluded cervical brown adipose tissue biopsies from humans for poor quality of planned western blots exploring IL10 pathway. The graphs were performed using GraphPad Prism 6 (GraphPad Software, Inc., La Jolla, CA).

5. Study approval

All animal studies were performed after approved by University of Campinas Ethics Committee, Campinas, São Paulo. All experimental procedures were conducted in accordance with guides of the Brazilian College of Animal Experimentation and the National Council of Animal Experimentation. The translational approach was conducted under an approved local ethic committee at Hospital de Clínicas da Unicamp, Campinas, São Paulo, Brazil, CAAE: 31865314.2.0000.5404. All volunteers consented previously to (¹⁸F)-FDG-PET/CT-scan imaging, hyperinsulinemic-euglycemic clamp, indirect calorimetry, blood collection and Roux en-Y Gastric Bypass (RYGB).

Conflict of interest

The authors have declared that no conflict of interest exists.

Author contributions

JCLJ, GFS and LAV conceived the study. JCLJ, GFS, AMA, JMG performed most experiments. ALR and MAM contributed with brown adipocytes experiments. JCLJ, DLF and HFC performed FLIM experiments. JCLJ, GFS, TIL, LRS and LAV analyzed and interpreted data. SCV and HFC performed transmission electronic microscopy. RSG and ERR performed bioinformatics analysis. JCLJ, JCP and BG selected and followed up obese patients. ILPB and CRC selected and followed up diabetic patients. JCP performed surgeries. JCLJ, SQB and CDR performed PET/CT analysis involving humans and mice. GRSS diagnosed and followed up patients with the mutations of IL10R. JCLJ and LAV wrote the manuscript. Competing interests: The authors declare no conflict of interest.

Funding

The study was supported by grants from the São Paulo Research Foundation (2013/07607-8) and Conselho Nacional de Pesquisa e Desenvolvimento Científico. INFABIC is co-funded by Fundação de Amparo a Pesquisa do Estado de São Paulo (FAPESP) (08/57906-3) and Conselho Nacional de Desenvolvimento Científico e Tecnológico (CNPq) (573913/2008-0).

Acknowledgments

The authors thank Erika Roman, Gerson Ferraz and Marcio Cruz for technical collaboration in the study. Joseane Morari for assistance in RNA extraction from whole blood. Rodrigo Carraro for assistance in one experiment involving animal treatment. Barbara J. Amorim for PET/CT evaluation. We thank the staff of the Life Sciences Core Facility (LaCTAD) from State University of Campinas (UNICAMP), for the Cell Biology analysis.

Appendix A. Supplementary data

Supplementary data to this article can be found online at <https://doi.org/10.1016/j.ebiom.2018.11.041>.

References

- Andreux PA, Williams EG, Koutnikova H, Houtkooper RH, Champy MF, Henry H, et al. Systems genetics of metabolism: the use of the BXD murine reference panel for multiscalar integration of traits. *Cell* 2012;150:1287–99.
- Andrews S. FastQC a quality control tool for high throughput sequence data; 2010.
- Arismendi-Morillo G. Electron microscopy morphology of the mitochondrial network in human cancer. *Int J Biochem Cell Biol* 2009;41:2062–8.
- Aune UL, Ruiz L, Kajimura S. Isolation and differentiation of stromal vascular cells to beige/brite cells. *J Vis Exp* 2013;73:50191.
- Belenguer P, Pellegrini L. The dynamin GTPase OPA1: more than mitochondria? *Biochim Biophys Acta* 2013;1833:176–83.
- Beraza N, Malato Y, Vander Borghet S, Liedtke C, Wasmuth HE, Dreano M, et al. Pharmacological IKK2 inhibition blocks liver steatosis and initiation of non-alcoholic steatohepatitis. *Gut* 2008;57:655–63.
- Blondin DP, Labbe SM, Noll C, Kunach M, Phoenix S, Guerin B, et al. Selective impairment of glucose but not fatty acid or oxidative metabolism in brown adipose tissue of subjects with type 2 diabetes. *Diabetes* 2015;64:2388–97.
- Bolger AM, Lohse M, Usadel B. Trimmomatic: a flexible trimmer for Illumina sequence data. *Bioinformatics* 2014;30:2114–20.
- Cavadas C, Aveleira CA, Souza GF, Velloso LA. The pathophysiology of defective proteostasis in the hypothalamus - from obesity to ageing. *Nat Rev Endocrinol* 2016;12:723–33.
- Chen KY, Cypess AM, Laughlin MR, Haft CR, Hu HH, Bredella MA, et al. Brown adipose reporting criteria in imaging STudies (BARCIST 1.0): recommendations for standardized FDG-PET/CT experiments in humans. *Cell Metab* 2016;24:210–22.
- Cintra DE, Pauli JR, Araujo EP, Moraes JC, de Souza CT, Milanski M, et al. Interleukin-10 is a protective factor against diet-induced insulin resistance in liver. *J Hepatol* 2008;48:628–37.
- Consortium G. The genotype-tissue expression (GTEx) project. *Nat Genet* 2013;45:580–5.
- Cypess AM, Lehman S, Williams G, Tal I, Rodman D, Goldfine AB, et al. Identification and importance of brown adipose tissue in adult humans. *N Engl J Med* 2009;360:1509–17.
- Dalla Via L, Garcia-Argaez AN, Martínez-Vazquez M, Grancara S, Martinis P, Toninello A. Mitochondrial permeability transition as target of anticancer drugs. *Curr Pharm Des* 2014;20:223–44.
- de Carvalho CP, Marin DM, de Souza AL, Pareja JC, Chaim EA, de Barros Mazon S, et al. GLP-1 and adiponectin: effect of weight loss after dietary restriction and gastric bypass in morbidly obese patients with normal and abnormal glucose metabolism. *Obes Surg* 2009;19:313–20.
- Del Dotto V, Mishra P, Vidoni S, Fogazza M, Maresca A, Caporali L, et al. OPA1 isoforms in the hierarchical organization of mitochondrial functions. *Cell Rep* 2017;19:2557–71.
- Demerath EW, Guo SS, Chumlea WC, Towne B, Roche AF, Siervogel RM. Comparison of percent body fat estimates using air displacement plethysmography and hydrodensitometry in adults and children. *Int J Obes Relat Metab Disord* 2002;26:389–97.
- Dickensheets HL, Freeman SL, Smith MF, Donnelly RP. Interleukin-10 upregulates tumor necrosis factor receptor type-II (p75) gene expression in endotoxin-stimulated human monocytes. *Blood* 1997;90:4162–71.
- Enerback S, Jacobsson A, Simpson EM, Guerra C, Yamashita H, Harper ME, et al. Mice lacking mitochondrial uncoupling protein are cold-sensitive but not obese. *Nature* 1997;387:90–4.
- Feldmann HM, Golozoubova V, Cannon B, Nedergaard J. UCP1 ablation induces obesity and abolishes diet-induced thermogenesis in mice exempt from thermal stress by living at thermoneutrality. *Cell Metab* 2009;9:203–9.
- Frayn KN. Calculation of substrate oxidation rates in vivo from gaseous exchange. *J Appl Physiol Respir Environ Exerc Physiol* 1983;55:628–34.
- Giorgi C, Baldassari F, Bononi A, Bonora M, De Marchi E, Marchi S, et al. Mitochondrial Ca(2+) and apoptosis. *Cell Calcium* 2012;52:36–43.
- Granneman JG. Renaissance of brown adipose tissue research: integrating the old and new. *Int J Obes Suppl* 2015;5:S7–S10.
- Granneman JG, Li P, Zhu Z, Lu Y. Metabolic and cellular plasticity in white adipose tissue I: effects of beta3-adrenergic receptor activation. *Am J Physiol Endocrinol Metab* 2005;289:E608–16.
- Grattagliano I, Russmann S, Diogo C, Bonfrate L, Oliveira PJ, Wang DQ, et al. Mitochondria in chronic liver disease. *Curr Drug Targets* 2011;12:879–93.
- Hong EG, Ko HJ, Cho YR, Kim HJ, Ma Z, Yu TY, et al. Interleukin-10 prevents diet-induced insulin resistance by attenuating macrophage and cytokine response in skeletal muscle. *Diabetes* 2009;58:2525–35.
- Hotamisligil GS. Foundations of immunometabolism and implications for metabolic health and disease. *Immunity* 2017;47:406–20.
- Hotamisligil GS. Inflammation, metaflammation and immunometabolic disorders. *Nature* 2017;542:177–85.
- Huang dW, Sherman BT, Lempicki RA. Systematic and integrative analysis of large gene lists using DAVID bioinformatics resources. *Nat Protoc* 2009;4:44–57.
- Hütter E, Unterluggauer H, Garedew A, Jansen-Dürr P, Gnaiger E. High-resolution respirometry—a modern tool in aging research. *Exp Gerontol* 2006;41:103–9.
- Ignacio-Souza LM, Bombassaro B, Pascoal LB, Portovedo MA, Razolli DS, Coope A, et al. Defective regulation of the ubiquitin/proteasome system in the hypothalamus of obese male mice. *Endocrinology* 2014;155:2831–44.
- Kaasik A, Safulina D, Zharkovsky A, Veksler V. Regulation of mitochondrial matrix volume. *Am J Physiol Cell Physiol* 2007;292:C157–63.
- Kazak L, Chouchani ET, Jedrychowski MP, Erickson BK, Shinoda K, Cohen P, et al. A creatine-driven substrate cycle enhances energy expenditure and thermogenesis in beige fat. *Cell* 2015;163:643–55.
- Kim HJ, Higashimori T, Park SY, Choi H, Dong J, Kim YJ, et al. Differential effects of interleukin-6 and -10 on skeletal muscle and liver insulin action in vivo. *Diabetes* 2004;53:1060–7.
- Koopman WJ, Verkaar S, Visch HJ, van der Westhuizen FH, Murphy MP, van den Heuvel LW, et al. Inhibition of complex I of the electron transport chain causes

- O2-.-mediated mitochondrial outgrowth. *Am J Physiol Cell Physiol* 2005;288: C1440–50.
- [36] Langmead B, Trapnell C, Pop M, Salzberg SL. Ultrafast and memory-efficient alignment of short DNA sequences to the human genome. *Genome Biol* 2009;10:R25.
- [37] Leitner BP, Huang S, Brychta RJ, Duckworth CJ, Baskin AS, McGehee S, et al. Mapping of human brown adipose tissue in lean and obese young men. *Proc Natl Acad Sci U S A* 2017;114:8649–54.
- [38] Li B, Dewey CN. RSEM: accurate transcript quantification from RNA-Seq data with or without a reference genome. *BMC Bioinformatics* 2011;12:323.
- [39] Lopez M. EJE PRIZE 2017: Hypothalamic AMPK: a golden target against obesity? *Eur J Endocrinol* 2017;176:R235–46.
- [40] Lopez M, Nogueiras R, Tena-Sempere M, Dieguez C. Hypothalamic AMPK: a canonical regulator of whole-body energy balance. *Nat Rev Endocrinol* 2016;12:421–32.
- [41] Marchesini G, Bugianesi E, Forlani G, Cerrelli F, Lenzi M, Manini R, et al. Nonalcoholic fatty liver, steatohepatitis, and the metabolic syndrome. *Hepatology* 2003;37: 917–23.
- [42] Martinez-Tellez B, Nahon KJ, Sanchez-Delgado G, Abreu-Vieira G, Llamas-Elvira JM, van Velden FHP, et al. The impact of using BARCIST 1.0 criteria on quantification of BAT volume and activity in three independent cohorts of adults. *Sci Rep* 2018;8:8567.
- [43] Mori MA, Thomou T, Boucher J, Lee KY, Lallukka S, Kim JK, et al. Altered miRNA processing disrupts brown/white adipocyte determination and associates with lipodystrophy. *J Clin Invest* 2014;124:3339–51.
- [44] Nakagome K, Dohi M, Okunishi K, Komagata Y, Nagatani K, Tanaka R, et al. In vivo IL-10 gene delivery suppresses airway eosinophilia and hyperreactivity by down-regulating APC functions and migration without impairing the antigen-specific systemic immune response in a mouse model of allergic airway inflammation. *J Immunol* 2005;174:6955–66.
- [45] Nishimura S, Manabe I, Takaki S, Nagasaki M, Otsu M, Yamashita H, et al. Adipose Natural Regulatory B Cells Negatively Control Adipose Tissue Inflammation. *Cell Metab* 2013;18:759–66.
- [46] Proudfoot AT. Aluminium and zinc phosphide poisoning. *Clin Toxicol (Phila)* 2009; 47:89–100.
- [47] Quiros PM, Ramsay AJ, Sala D, Fernandez-Vizarra E, Rodriguez F, Peinado JR, et al. Loss of mitochondrial protease OMA1 alters processing of the GTPase OPA1 and causes obesity and defective thermogenesis in mice. *EMBO J* 2012;31:2117–33.
- [48] Rachid B, van de Sande-Lee S, Rodovalho S, Folli F, Beltrami GC, Morari J, et al. Distinct regulation of hypothalamic and brown/beige adipose tissue activities in human obesity. *Int J Obes (Lond)* 2015;39:1515–22.
- [49] Ramalho AF, Bombassaro B, Dragano NR, Solon C, Morari J, Fioravante M, et al. Dietary fats promote functional and structural changes in the median eminence blood/spinal fluid interface—the protective role for BDNF. *J Neuroinflammation* 2018;15:10.
- [50] Ramseyer VD, Granneman JG. Adrenergic regulation of cellular plasticity in brown, beige/brite and white adipose tissues. *Adipocyte* 2016;5:119–29.
- [51] Rasola A, Bernardi P. Mitochondrial permeability transition in ca(2+)-dependent apoptosis and necrosis. *Cell Calcium* 2011;50:222–33.
- [52] Rennick D, Davidson N, Berg D. Interleukin-10 gene knock-out mice: a model of chronic inflammation. *Clin Immunol Immunopathol* 1995;76:S174–8.
- [53] Rennick DM, Fort MM. Lessons from genetically engineered animal models. XII. IL-10 deficient (IL-10(-/-)) mice and intestinal inflammation. *Am J Physiol Gastrointest Liver Physiol* 2000;278:G829–33.
- [54] Rodovalho S, Rachid B, De-Lima-Junior JC, van de Sande-Lee S, Morari J, Carvalho HM, et al. Impairment of body mass reduction-associated activation of brown/beige adipose tissue in patients with type 2 diabetes mellitus. *Int J Obes (Lond)* 2017;41:1662–8.
- [55] Schindelin J, Arganda-Carreras I, Frise E, Kaynig V, Longair M, Pietzsch T, et al. Fiji: an open-source platform for biological-image analysis. *Nat Methods* 2012;9:676–82.
- [56] Schrauwen P, van Marken Lichtenbelt WD. Combatting type 2 diabetes by turning up the heat. *Diabetologia* 2016;59:2269–79.
- [57] Shabalina IG, Ost M, Petrovic N, Vrbacky M, Nedergaard J, Cannon B. Uncoupling protein-1 is not leaky. *Biochim Biophys Acta* 2010;1797:773–84.
- [58] Sidossis L, Kajimura S. Brown and beige fat in humans: thermogenic adipocytes that control energy and glucose homeostasis. *J Clin Invest* 2015;125:478–86.
- [59] Simcox J, Geoghegan G, Maschek JA, Bensard CL, Pasquali M, Miao R, et al. Global analysis of plasma lipids identifies liver-derived acylcarnitines as a fuel source for brown fat thermogenesis. *Cell Metab* 2017;26:509–22 e506.
- [60] Smolen JS, Landewe R, Bijlsma J, Burmester G, Chazdionysiou K, Dougados M, et al. EULAR recommendations for the management of rheumatoid arthritis with synthetic and biological disease-modifying antirheumatic drugs: 2016 update. *Ann Rheum Dis* 2017;76:960–77.
- [61] Sood A, Jeyaraju DV, Prudent J, Caron A, Lemieux P, McBride HM, et al. A Mitofusin-2-dependent inactivating cleavage of Opa1 links changes in mitochondria cristae and ER contacts in the postprandial liver. *Proc Natl Acad Sci U S A* 2014;111: 16017–22.
- [62] Tahari AK, Chien D, Azadi JR, Wahl RL. Optimum lean body formulation for correction of standardized uptake value in PET imaging. *J Nucl Med* 2014;55:1481–4.
- [63] Ungar B, Kopylov U. Advances in the development of new biologics in inflammatory bowel disease. *Ann Gastroenterol* 2016;29:243–8.
- [64] van den Berg SM, van Dam AD, Rensen PC, de Winther MP, Lutgens E. Immune Modulation of Brown(ing) Adipose Tissue in Obesity. *Endocr Rev* 2017;38:46–68.
- [65] van Exel E, Gussekloo J, de Craen AJ, Frolich M, Der Wiel Bootsma-Van, Westendorp RG, et al. Low production capacity of interleukin-10 associates with the metabolic syndrome and type 2 diabetes : the Leiden 85-Plus Study. *Diabetes* 2002;51: 1088–92.
- [66] van Marken Lichtenbelt WD, Vanhommerig JW, Smulders NM, Drossaerts JM, Kemerink GJ, Bouvy ND, et al. Cold-activated brown adipose tissue in healthy men. *N Engl J Med* 2009;360:1500–8.
- [67] Velloso LA, Folli F, Saad MJ. TLR4 at the crossroads of nutrients, gut microbiota, and metabolic inflammation. *Endocr Rev* 2015;36:245–71.
- [68] Vidoni S, Zanna C, Rugolo M, Sarzi E, Lenaers G. Why mitochondria must fuse to maintain their genome integrity. *Antioxid Redox Signal* 2013;19:379–88.
- [69] Vijgen GH, Bouvy ND, Teule GJ, Brans B, Hoeks J, Schrauwen P, et al. Increase in brown adipose tissue activity after weight loss in morbidly obese subjects. *J Clin Endocrinol Metab* 2012;97:E1229–33.
- [70] Villarroya F, Cereijo R, Villarroya J, Giral M. Brown adipose tissue as a secretory organ. *Nat Rev Endocrinol* 2017;13:26–35.
- [71] Virtanen KA, Lidell ME, Orava J, Heglind M, Westergren R, Niemi T, et al. Functional brown adipose tissue in healthy adults. *N Engl J Med* 2009;360:1518–25.
- [72] Zanna C, Ghelli A, Porcelli AM, Karbowski M, Youle RJ, Schimpf S, et al. OPA1 mutations associated with dominant optic atrophy impair oxidative phosphorylation and mitochondrial fusion. *Brain* 2008;131:352–67.